Journal of Microelectronics and Electronic Packaging (2011) **8**, 121-128

ISSN: 1551-4897

A Novel Design of Substrate Integrated Waveguide (SIW) E-Plane Inductive Strip Filter Implemented Using LTCC

Ehab Abousaif, Aicha Elshabini, and Fred Barlow*

***Abstract*—Low-temperature cofired ceramic (LTCC) was used for a novel band-pass filter design. The filter is based on metallic strips parallel to the E-plane and mounted in a substrate-integrated waveguide (SIW). A new iterative technique based on the variation principle was used to obtain the inductive reactance of equivalent T-network of the metallic strip. The design method of the filter was derived by applying the equivalent network of the metallic strip to the usual method of the filter design. A set of curves relating the various filter parameters is introduced. This filter was designed such that it is electromagnetically isolated inside the SIW and excited using grounded coplanar waveguide (GCPW) to SIW transitions; therefore, it can be easily integrated with MMICs. The design steps are explained and verified by examples and results. Three-dimensional electromagnetic field modeling and simulation was carried out using a high frequency structure simulator (HFSS). A comparison between different types of SIW is presented showing the resulting S-parameter curves for each case. By following the design steps, similar filters for various frequency bands using any dielectric material can be easily designed.**

***Keywords*—Filter design, low temperature co-fired ceramic (LTCC), substrate-integrated waveguide (SIW), variation principle**

Introduction

Substrate-integrated waveguide (SIW) filters using LTCC is one solution that makes the waveguide filters successful in microelectronic applications. However, most of these filters use cavity resonator or ridge techniques [1-10]. In this paper, an SIW E-plane inductive strip filter using an LTCC substrate is introduced, as shown in Fig. 1. The main concept of that filter is the use of metallic diaphragms (strips with small thickness) with certain widths mounted inside the waveguide parallel to the electric field plane with specific spacing between them. These metallic strips are considered as discontinuities inside the waveguide that will generate higher order modes. Since these metallic strips are parallel to the E-plane, H_{n0} will be the only type of the higher order modes that will be generated; therefore the equivalent network of these metallic strips is inductive reactance, and hence the name inductive strip filter. The advantages of that filter over other SIW filters are the straightforward design criterion, the ease of fabrication with low cost, and the relatively small size. This filter can be used efficiently in the following frequency bands: X-band, Ku-band, K-band, and Ka-band. Lower than the X-band, the filter becomes relatively large, and higher than Ka-band, the widths of the strips become too small to be manufactured in most cases.

A new method of design for the planar circuit filter with inductive strip is presented. First, the equivalent T-network of an inductive strip inserted in the middle of a waveguide parallel to the E-plane was represented [11]. The equivalent circuit of the inductive strip was calculated using an iterative technique based on the variation principle [12]. A MATLAB program was used to generate a set of curves that relate the inductive strip width to the equivalent circuit parameters. The design method of the filter was derived by applying the equivalent circuit of the inductive strip to the usual method of filter design using K-inverters [13].

An example of a fourth order, maximally flat band pass filter in KU-band is presented in this work using 9K7 green-tape LTCC [14]. Curves and values calculated by the design method were introduced. The input and output excitation ports for the LTCC substrate were optimized. Modeling, simulation, and results of the designed filter were carried out using HFSS.

Design Methodology

A. Equivalent T-Network

The first step of the design procedure is the calculation of the equivalent T-network of a metallic strip placed in the middle of a waveguide parallel to the E-plane. Fig. 2 shows the geometry of the metallic strip.

By using the Z-parameter equivalent circuit, the T-network can be obtained as shown in Fig. 3, where $Z_s \equiv jX_s$ and $Z_p \equiv jX_p$. The T-network can be redrawn to become a symmetrical network, as shown in Fig. 4. Now, the Z-parameter can be obtained from one port only (one half circuit).

For one half circuit, the open circuit impedance is $Z_{OC} = Z_{11} + Z_{12}$ and the short circuit impedance is $Z_{SC} = Z_{11} - Z_{12}$. The open circuit boundary is equivalent to a magnetic wall at the T_0-plane ($Z = W/2$), and the short circuit boundary is equivalent to an electric wall at the T_0-plane.

The expressions of Z_s and Z_p can be easily obtained from Z_{OC} and Z_{SC} as follows:

$$jX_s \equiv Z_s = Z_{SC} \tag{1}$$

$$jX_p \equiv Z_p = \frac{1}{2(Z_{OC} - Z_{SC})} \tag{2}$$

Manuscript received October 2011 and accepted January 2012.

Department of Electrical Engineering, University of Idaho, Moscow, Idaho, 83844

*Corresponding author; email: fbarlow@uidaho.edu

doi:10.4071/imaps.304

The expressions of Z_{OC} and Z_{SC} can be obtained using the variation principle.

B. Variation Principle

The second step of the design procedure is the application of the variation principle.

Since the discontinuity in the waveguide due to the inductive strip is uniform along the y axis, the only types of higher order modes excited at the strip are H_{n0} modes [12]. The field in the region $Z \leq 0$ will be given by an expansion in terms of an infinite set of H_{n0} modes as follows:

$$E_y = a_1\phi_1 e^{-\Gamma_1 Z} + R_1 a_1 \phi_1 e^{\Gamma_1 Z} + \sum_{n=3,5,\ldots}^{\infty} a_n \phi_n e^{\Gamma_n Z} \quad (3)$$

$$H_x = -Y_1 a_1 \phi_1 e^{-\Gamma_1 Z} + R_1 Y_1 a_1 \phi_1 e^{\Gamma_1 Z} + \sum_{n=3,5,\ldots}^{\infty} Y_n a_n \phi_n e^{\Gamma_n Z} \quad (4)$$

where,

$$\phi_n = \sin\left(\frac{n\pi x}{a}\right) \quad (5)$$

$$\Gamma_n^2 = \left(\frac{n\pi}{a}\right)^2 - k_0^2 \quad (6)$$

$$Y_n = \left(\frac{-j\Gamma_n}{k_0}\right) Y_0 \quad (7)$$

$k_0 = \dfrac{2\pi}{\lambda_0} \equiv$ free space wave number,

$Y_0 = \dfrac{1}{\eta_0} \equiv$ characteristic admittance of free space, and

$R_1 \equiv$ reflection coefficient.

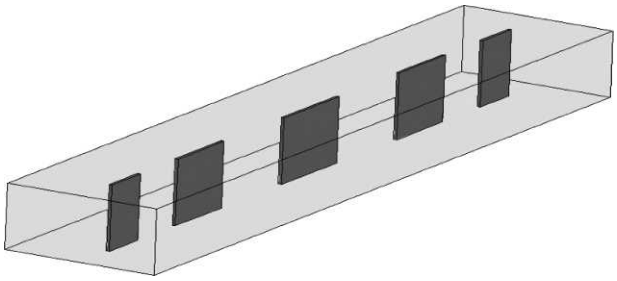

Fig. 1. Waveguide inductive strip filter.

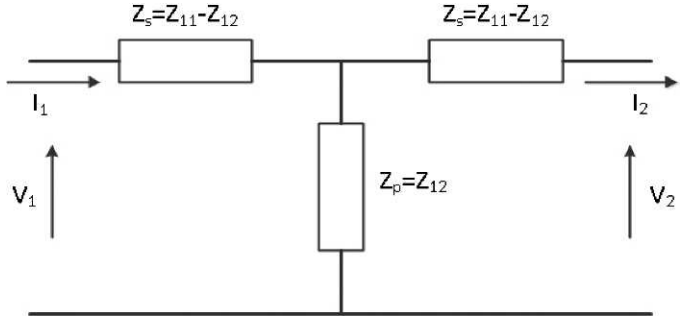

Fig. 3. Z-parameter T-network equivalent circuit of the inductive strip.

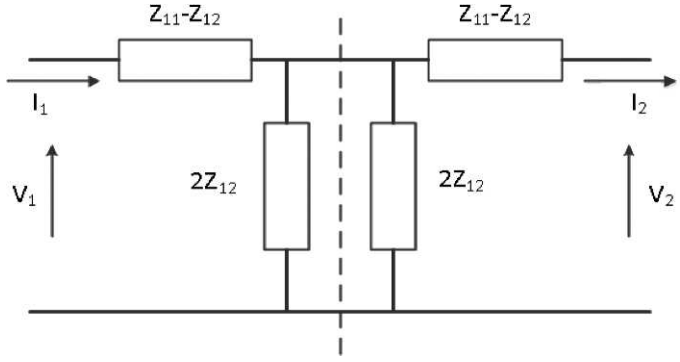

Fig. 4. Symmetrical Z-parameter T-network equivalent circuit of the inductive strip.

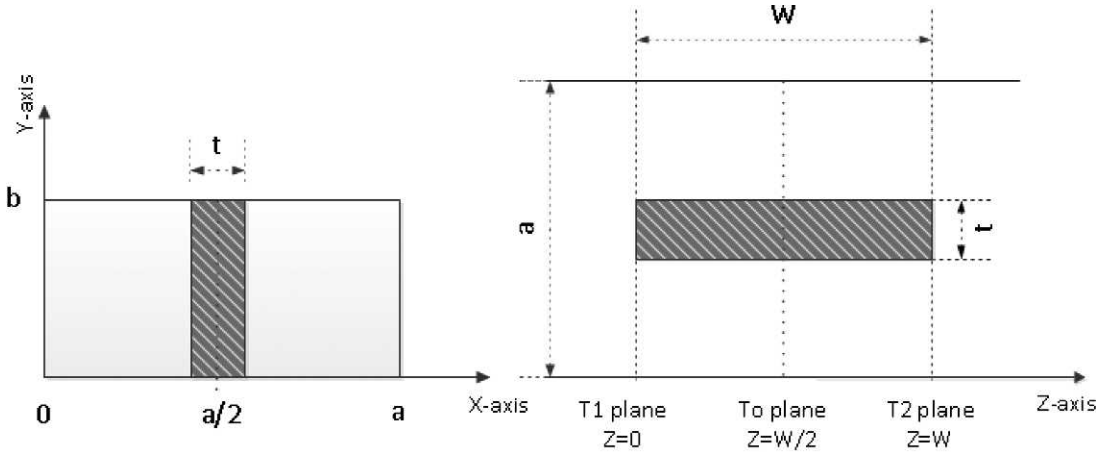

Fig. 2. The geometry of metallic strip placed in the middle of a waveguide parallel to the E-plane. The left figure shows the end view and the right figure shows the top view.

For the case of magnetic wall, at $Z = W/2$, the transverse magnetic field vanishes. Thus the expression of the field in the region $0 \le Z \le W/2$ will be as follows:

$$E_y = \sum_{n=1,3,\ldots}^{\infty} b_n \psi_n(x) \cosh \gamma_n \left(Z - \frac{W}{2} \right) \tag{8}$$

$$H_x = \sum_{n=1,3,\ldots}^{\infty} Y_{0n} b_n \psi_n(x) \sinh \gamma_n \left(Z - \frac{W}{2} \right) \tag{9}$$

where,

$$\psi_n(x) = \sin\left(\frac{2n\pi x}{a-t} \right) \tag{10}$$

$$\gamma_n^2 = \left(\frac{2n\pi}{a-t} \right)^2 - k_0^2 \tag{11}$$

$$Y_{0n} = \frac{-j\gamma_n}{k_0} Y_0 \tag{12}$$

By applying the continuity of the transverse fields at $Z = 0$, the result will be as follows:

$$(1 - R_1) Y_1 a_1 \phi_1 - \sum_{n=3,5,\ldots}^{\infty} a_n Y_n \phi_n = \sum_{n=1,3,\ldots}^{\infty} b_n Y_{0n} \psi_n \sinh\left(\gamma_n \frac{W}{2} \right) \tag{13}$$

where $(1 - R_1) Y_1 a_1 = I_1 = (Z_{\mathrm{OC}})^{-1} V_1$

Let the transverse electric field at $Z = 0$ be $\varepsilon(x)$. By Fourier analysis:

$$V_1 = \frac{4}{a} \int_0^{\frac{a}{2}} \varepsilon(x') \phi_1(x') dx' \tag{14}$$

$$a_n = \frac{4}{a} \int_0^{\frac{a}{2}} \varepsilon(x') \phi_1(x') dx' \tag{15}$$

$$b_n = \frac{4}{(a-t)\cosh\left(\gamma_n \frac{W}{2}\right)} \int_0^{\frac{a-t}{2}} \varepsilon(x') \psi_n(x') dx' \tag{16}$$

A variational expression for $(Z_{\mathrm{OC}})^{-1}$can be obtained by substituting the integral expressions from eqs. (14), (15), and (16) into (13), multiplying eq. (13) by $\varepsilon(x)$, integrating over the waveguide half width

$$\left(\int_0^{\frac{a}{2}} \right),$$

and dividing both sides by

$$\left(\int_0^{\frac{a}{2}} \varepsilon \phi_1 dx \right)^2.$$

The expression will be as follows:

$$(Z_{\mathrm{OC}})^{-1} = \frac{-j \int_0^{\frac{a}{2}} \int_0^{\frac{a}{2}} \varepsilon(x) \varepsilon(x') G_1(x|x') dx dx'}{\left[\int_0^{\frac{a}{2}} \varepsilon(x) \phi_1(x) dx \right]^2} \tag{17}$$

where,

$$-jG_1(x|x') = \sum_{n=3,5,\ldots}^{\infty} Y_n \phi_n(x) \phi_n(x') + \frac{a}{a-t} \sum_{n=1,3,\ldots}^{\infty} Y_{0n} \psi_n(x) \psi_n(x') \tanh\left(\gamma_n \frac{W}{2} \right) \tag{18}$$

For the case of electric wall, at $Z = W/2$, the transverse electric field vanishes. A similar procedure to the magnetic wall can be done, and yields the following equations:

$$(Z_{\mathrm{SC}})^{-1} = \frac{-j \int_a^{a/2} \int_a^{a/2} \varepsilon(x) \varepsilon(x') G_2(x|x') dx dx'}{\left[\int_0^{a/2} \varepsilon(x) \phi_1(x) dx \right]^2} \tag{19}$$

where,

$$-jG_2(x|x') = \sum_{n=3,5,\ldots}^{\infty} Y_n \phi_n(x) \phi_n(x') + \frac{a}{a-t} \sum_{n=1,3,\ldots}^{\infty} Y_{0n} \psi_n(x) \psi_n(x') \coth\left(\gamma_n \frac{W}{2} \right) \tag{20}$$

A convenient choice for the transverse electric field $\varepsilon(x)$ is an expansion in terms of the orthogonal set of functions $\psi_m(x)$ as follows:

$$\varepsilon(x) = \sum_{m=1,3,\ldots}^{M} b_m \psi_m(x) \tag{21}$$

The parameter M is chosen according to the accuracy required. The results obtained from the design example in the next section show that a two term approximation is sufficient for the determination of the Z parameters.

By substituting the two term expansion from eq. (21) into eq. (17) and simplifying, the evaluation of $(Z_{\mathrm{OC}})^{-1}$ reduces to the evaluation of (2×2) determinants as follows:

$$(Z_{\mathrm{OC}})^{-1} \begin{vmatrix} 1 & 1 \\ \frac{h_{31}}{p_{11}p_{31}} - \frac{h_{11}}{p_{11}^2} & \frac{h_{33}}{p_{31}^2} - \frac{h_{13}}{p_{11}p_{31}} \end{vmatrix} = -j \begin{vmatrix} \frac{h_{11}}{p_{11}^2} & \frac{h_{13}}{p_{11}p_{31}} \\ \frac{h_{31}}{p_{11}p_{31}} - \frac{h_{11}}{p_{11}^2} & \frac{h_{33}}{p_{31}^2} - \frac{h_{13}}{p_{11}p_{31}} \end{vmatrix} \tag{22}$$

where,

$$p_{mn} = \int_0^{\frac{a-t}{2}} \psi_m(x) \phi_n(x) dx = \frac{\left(\frac{2m\pi}{a-t} \right) \left(\sin\left(\frac{n\pi t}{2a} + \frac{\pi}{2} \right) \right)}{\frac{4m^2\pi^2}{(a-t)^2} - \frac{n^2\pi^2}{a^2}} \tag{23}$$

$$h_{11} = j \sum_{n=3,5,\ldots}^{\infty} Y_n p_{1n}^2 + j \frac{a(a-t)}{16} \left[Y_{01} \tanh\left(\gamma_1 \frac{W}{2} \right) \right] \tag{24}$$

$$h_{33} = \sum_{n=3,5,\ldots}^{\infty} Y_n p_{3n}^2 + j \frac{a(a-t)}{16} \left[Y_{03} \tanh\left(\gamma_3 \frac{W}{2} \right) \right] \tag{25}$$

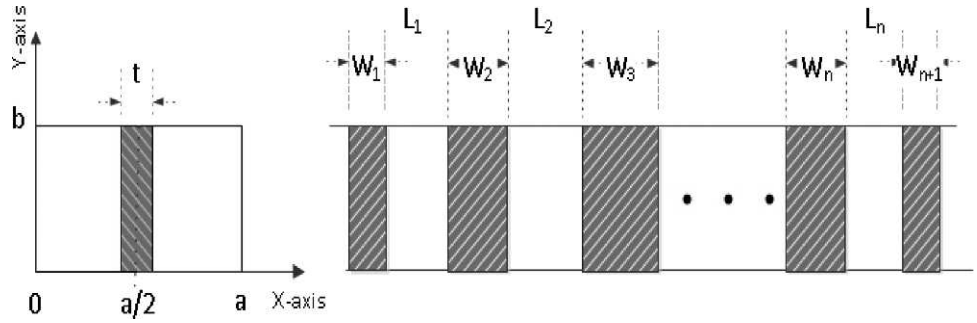

Fig. 5. The *n*th order waveguide inductive strip band pass filter.

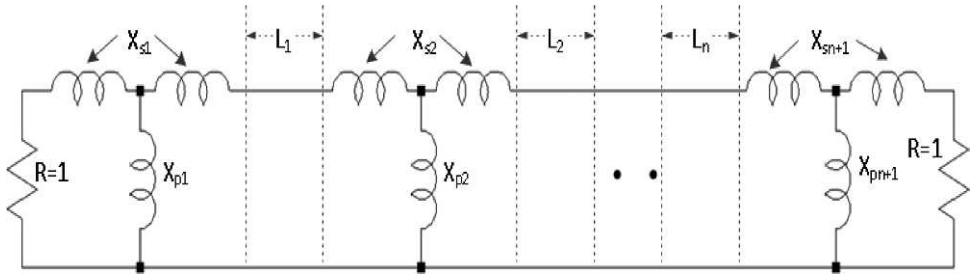

Fig. 6. T-equivalent network of the *n*th order waveguide inductive strip band pass filter.

$$h_{13} = h_{31} = j \sum_{n=3,5,\ldots}^{\infty} Y_n p_{1n} p_{3n} \tag{26}$$

The same equations are valid for the calculation of $(Z_{SC})^{-1}$ by replacing Z_{OC} with Z_{SC} in eq. (22) and replacing the tanh function with a coth function in eqs. (24), (25), and (26).

By selecting the desired working frequency, the waveguide width (a), and the inductive strip thickness (t), eqs. (1), (2), and (22-26) establish a relation between the strip width (W) and the T-network parameters (X_p and X_s), which can be given in a curve format using MATLAB. Curves are shown in the next section for a fourth order maximally flat band pass filter (BPF) in the KU-frequency band.

C. Band-Pass Filter Design

The third step of the design procedure is the filter design. The method of design based on the impedance K-inverters [13]. Fig. 5 shows an *n*th-order inductive strip BPF. The widths of the strips are represented by W_1 through W_{n+1} and the spacing between the strips is represented by L_1 through L_n. Fig. 6 shows the equivalent network of the filter.

The symmetrical T-reactance connected to the transmission line acts as an impedance *K*-inverter network. Therefore, the equivalent network in Fig. 6 can be transformed to give the equivalent *K*-inverter network in Fig. 7.

The values of the *K*-inverters can be easily calculated using the following equations [13]:

$$K_{01} = \left(\frac{x_1 \omega}{g_0 g_1}\right)^{1/2} \tag{27}$$

$$K_{j,j+1} = \omega \left(\frac{x_j x_{j+1}}{g_j g_{j+1}}\right)^{1/2} \tag{28}$$

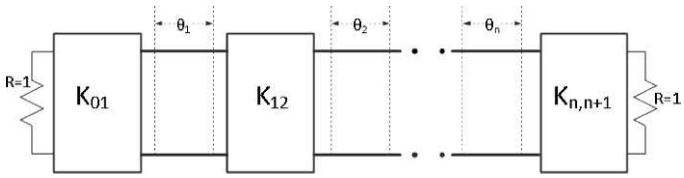

Fig. 7. *K*-inverter equivalent network of the *n*th order waveguide inductive strip band pass filter.

$$K_{n,n+1} = \left(\frac{x_n \omega}{g_n g_{n+1}}\right)^{1/2} \tag{29}$$

where $g_0, g_1, \ldots, g_{n+1}$ are the low pass filter prototype g values, ω is the fractional bandwidth, and x_j are the slope reactance parameters calculated at the center frequency of the filter.

The values of x_j can be chosen arbitrarily according to the filter design. In the case of waveguide filters, it is convenient to choose x_j for half-wavelength guided transmission line as follows:

$$x_j = \frac{\pi}{2}\left(\frac{\lambda_g}{\lambda_0}\right)^2 \tag{30}$$

$$\lambda_g = \frac{\lambda_0}{\left[1 - \left(\frac{\lambda_0}{2a}\right)^2\right]^{1/2}} \tag{31}$$

where λ_g is the guided wavelength.

Fig. 8 shows the relations between the *K*-inverter values and the T-reactance values (X_p and X_s). These relations are given by the following equations [13]:

$$K_{j-1,j} = \left|\tan\left(\frac{1}{2}\phi_j + \tan^{-1} X_{sj}\right)\right| \tag{32}$$

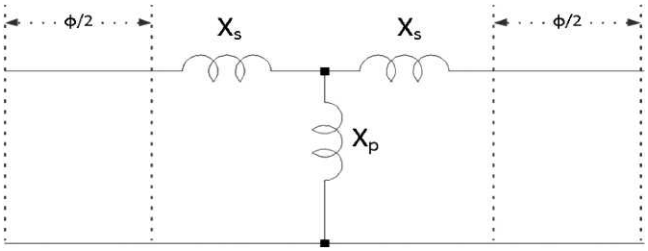

Fig. 8. *K*-inverter T-network relation.

$$\phi_j = -\tan^{-1}\left(2X_{pj} + X_{sj}\right) - \tan^{-1}X_{sj} \tag{33}$$

Using eqs. (32) and (33) with the resulting relations between W, X_p, and X_s from the variation principle, an iterative technique can be built to get the value of the strip width (W) associated with each K-inverter value.

Once the values of W, X_p, and X_s are obtained, the following equation is used to obtain the values of θ_j:

$$\phi_j = \pi + \frac{1}{2}\left(\phi_j + \phi_{j+1}\right) \tag{34}$$

The spacing between the strips is given by:

$$L_j = \frac{\theta_j}{2\pi}\lambda_g \tag{35}$$

Design Example

A. Filter Specification

A fourth order, maximally flat, KU-band pass filter is introduced as an example to demonstrate the design procedure and verify the design methodology.

The filter has a center frequency of 14 GHz, and a fractional bandwidth of 3%. The LTCC substrate is based on 9K7 greentape, with a dielectric constant of 7.1 and a loss tangent of 0.001 at 14 GHz frequency [14]. The substrate-integrated waveguide has a width (a) of 5.92 mm and a height (b) of 3 mm. The metallic strip thickness (t) is 0.2 mm.

B. Design Outcomes

For a fourth order maximally flat band pass filter, the g values were given as [13]:

$$g_0 = 1 = g_5, g_1 = 0.7654 = g_4, \text{and } g_2 = 1.848 = g_3$$

Using eqs. (27) through (31), the values of the K-inverters were obtained as:

$$K_{01} = 0.337594 = K_{45}$$
$$K_{12} = 0.073347 = K_{34}$$
$$K_{23} = 0.047204$$

Using eqs. (1), (2), and (22) through (26), a MATLAB program was used to generate two curves that relate the strip width (W) to the T-reactance parameters (X_s) and (X_p). Fig. 9 and Fig. 10 show these relations.

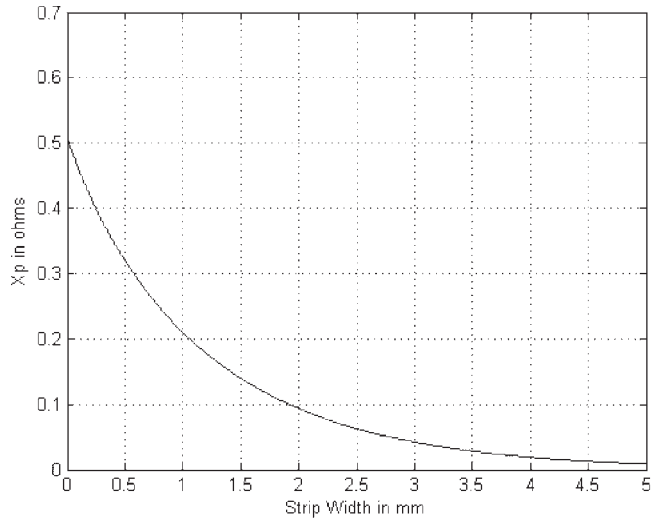

Fig. 9. X_p versus W.

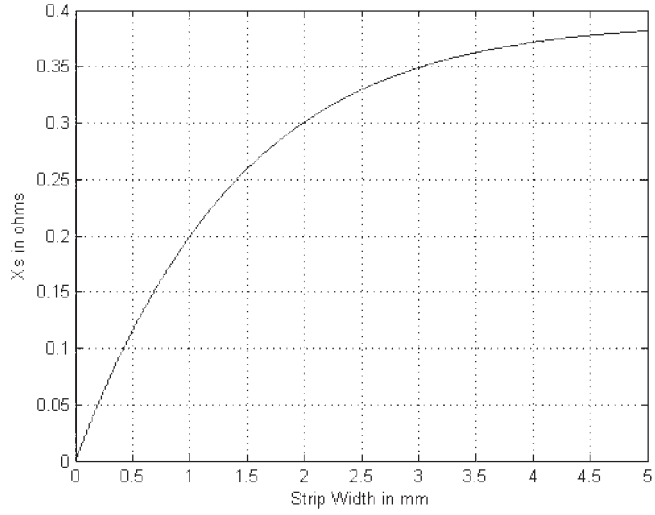

Fig. 10. X_s versus W.

An iterative process was built using eqs. (32) and (33). Along with the MATLAB results, the strip widths were obtained as:

$$W_1 = 0.355 \text{ mm} = W_5$$
$$W_2 = 2.318 \text{ mm} = W_4$$
$$W_3 = 2.889 \text{ mm}$$

Using eqs. (34) and (35), the values of the strip spacing were obtained as:

$$L_1 = 4.04 \text{ mm} = L_4$$
$$L_2 = 4.098 \text{ mm} = L_3$$

The values of the strip widths have to be modified to compensate for the fringing effect around the strip edges. Due to this fringing effect, the strips appear to be wider than their original widths. A reduction factor must be added to the values of the strip widths.

A reduction factor of 1% of the strip width was found to be reasonable to compensate for the fringing effect. The modified strip widths were found to be as follows:

$$W_1 = W_{1_{\text{old}}} - 0.01W_{1_{\text{old}}} = 0.35 \text{ mm} = W_5$$
$$W_2 = W_{2_{\text{old}}} - 0.01W_{2_{\text{old}}} = 2.3 \text{ mm} = W_4$$
$$W_3 = W_{3_{\text{old}}} - 0.01W_{3_{\text{old}}} = 2.86 \text{ mm}$$

Modeling, Simulation, and Results

A. Filter Modeling

The high frequency structure simulator (HFSS) was used to model and simulate the designed filter.

The simulation was made using various types of SIW according to the construction of the waveguide walls. The first type was using solid metallic-wall waveguide, which can be made by plating the substrate sides with metal. Fig. 11 shows the model of the solid metallic wall SIW. These solid walls can be easily replaced by via holes with pitch distance less than one-tenth of the guided wavelength such that they act as a solid wall for the EM-wave.

According to the construction of via holes, other types of SIW were formulated. The second type was constructed using one row of via holes of 0.2 mm diameter and 0.6 mm pitch distance between successive via holes. Fig. 12 shows the model of this type.

The third type was constructed using the same one row of via holes in addition to metallic traces of 0.2 mm width that connected the via catch pads for each layer of the green-tape. Fig. 13 shows the model of the third type. The purpose of these metallic traces is to avoid any vertical misalignment in via holes among the layers during filter fabrication.

The fourth type was constructed using two rows of staggered via holes of 0.2 mm diameter and 0.6 mm pitch distance between each two successive via holes. Fig. 14 shows the model of that type. Adding metallic traces for each layer of the previous model gave the fifth type of the SIW, as shown in Fig. 15.

A grounded coplanar waveguide (GCPW) was designed to have 50 Ω characteristic impedance and was used as the excitation port of the filter. The height of the GCPW substrate was designed to have two green-tape 9K7X layers.

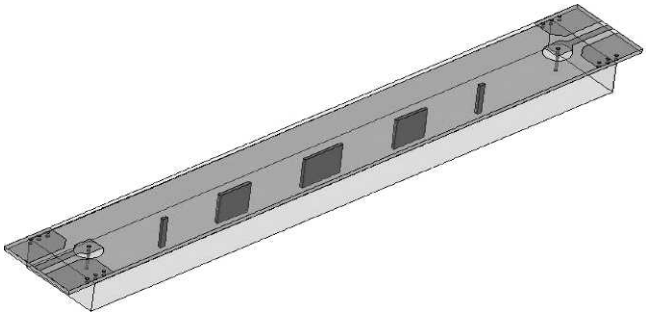

Fig. 11. Solid metallic wall filter model in HFSS.

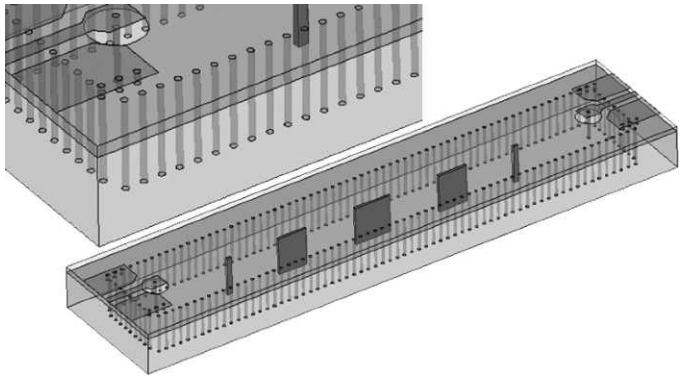

Fig. 12. One row of via holes filter model in HFSS.

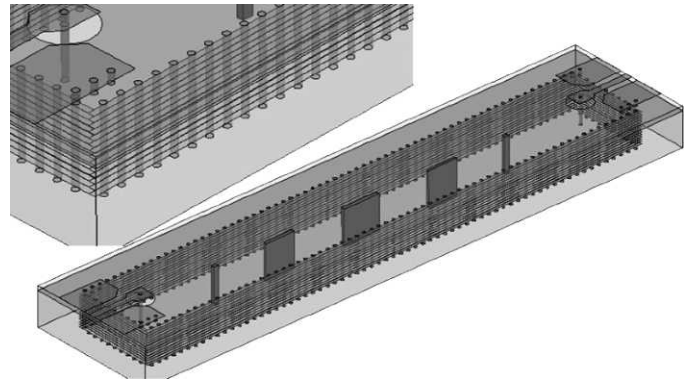

Fig. 13. One row of via holes with metallic traces filter model in HFSS.

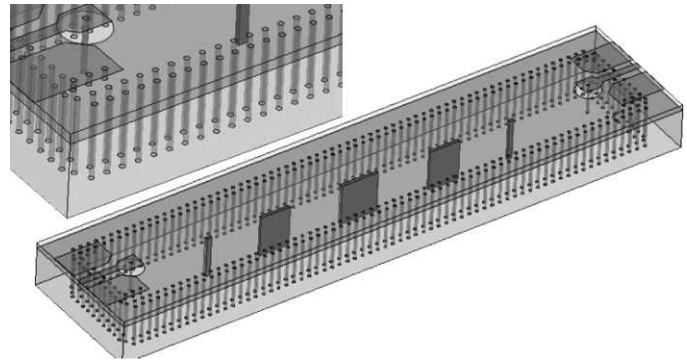

Fig. 14. Two rows of staggered via holes filter model in HFSS.

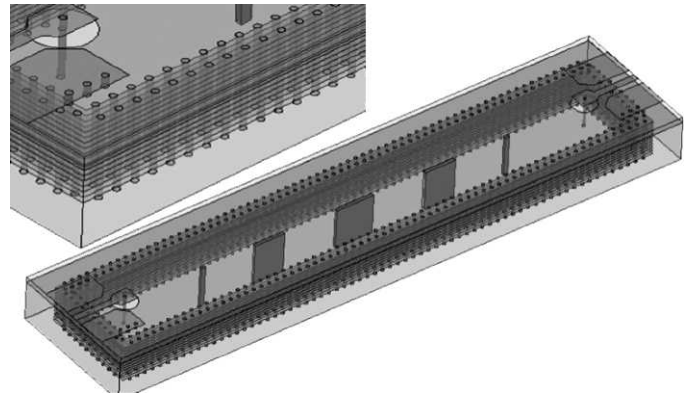

Fig. 15. Two rows of staggered via holes with metallic traces filter model in HFSS.

A transition from GCPW to SIW was designed using a via hole of 0.2 mm diameter and 2.2 mm length that probed the waveguide in a center position and short distance of 2 mm to the waveguide wall. This type of excitation offers ground-signal-ground connections, which is suitable for measurements and also suitable for wire-bonding, in case of integration with active elements in MMICs. Also, it can be easily transferred to a microstrip with the same probing via hole. The 50 Ω characteristic impedance of the GCPW gives the ability to attach the standard types of connectors to the excitation ports of the filter, in case of standalone usage.

The height of the SIW was designed to have 15 green-tape 9K7X layers. A total of 17 green-tape layers were used to formulate the whole substrate. The actual length of the SIW was 40 mm and the actual width was 5.92 mm.

B. Simulation Results

The results were based on simulation processes done by HFSS. A comparison was done between the various types of SIW constructions based on the simulated S-parameters of the designed filter.

Fig. 16 shows the simulated S-parameters of the first type, solid metallic wall waveguide, filter. The results show an insertion loss of less than –1 dB in the pass band, a shape factor better than 2.5:1 at 30:3 dB, and S_{11} less than –26 dB in the pass band.

Fig. 17 shows the simulated S-parameters of the second type filter, one row of via holes. The results show an insertion loss of less than –1 dB in the pass band, S_{11} less than –26 dB in the pass band; but the shape factor was affected. It became 2.6:1 at 30:3 dB. Also, there is a small shift in the center frequency with a value of 0.2%. These effects occurred due to the conversion of the solid metallic walls of the waveguide into a via fence. Thus, there was no complete isolation of the field inside the waveguide, but the results still show a good filter shape.

Fig. 18 shows a comparison between one row and two rows staggered via walls. It can be shown that the shift of the center frequency was slightly compensated for by adding the second row of via holes. Fig. 19 shows a comparison between two rows and two rows with metallic traces. It can be shown that the two types had the same response. But as was said previously, adding these metallic traces avoids the effect of misalignment between via holes.

Depending on these results, the optimum way to design a substrate-integrated waveguide is by using two rows of staggered via holes connected with metallic traces for each layer.

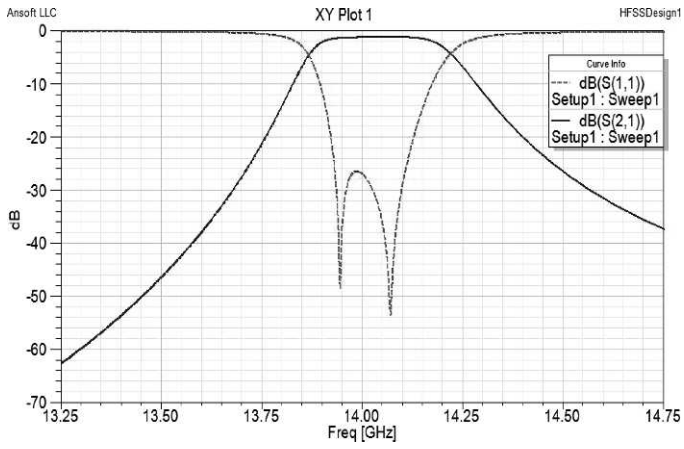

Fig. 16. Simulated S-parameters of solid metallic wall filter.

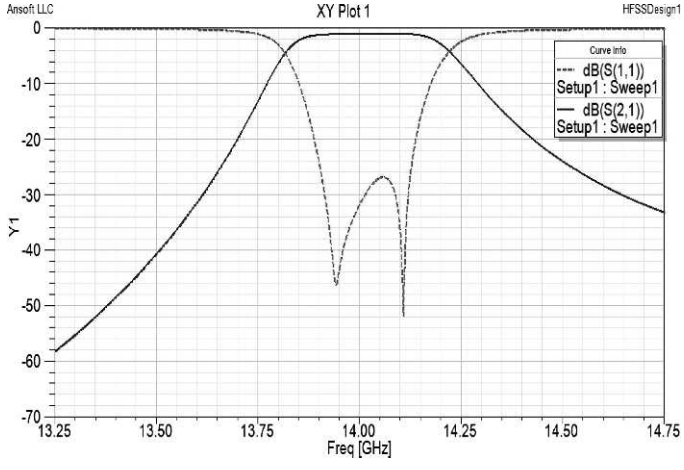

Fig. 17. Simulated S-parameters of one row of via holes filter.

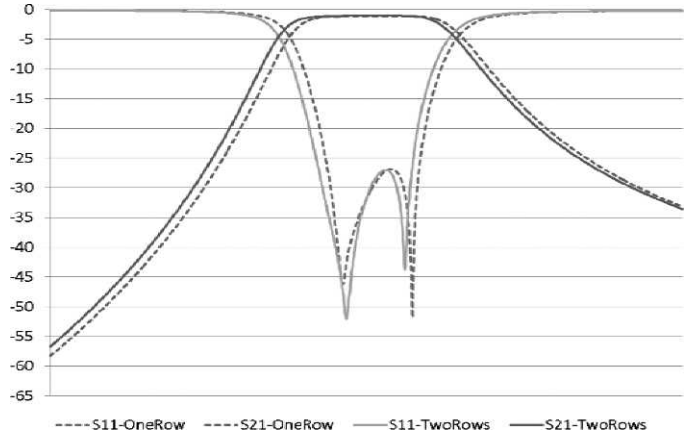

Fig. 18. Comparison between the simulated S-parameters of one row of via holes and two rows of staggered via holes filters.

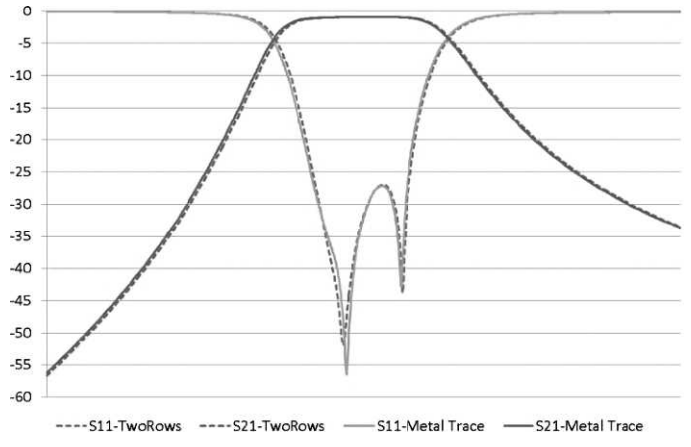

Fig. 19. Comparison between the simulated S-parameters of two rows of staggered via holes and two rows of staggered via holes with metallic traces filters.

Conclusion

A novel design for SIW filter implemented using LTCC was introduced in this paper. The variation principle was used to design the filter. The design procedure is clear and can be followed easily. HFSS was used to model and simulate different types of the designed SIW filter. The small size of the filter and the GCPW excitation ports make this filter appropriate to be integrated with MMICs. The simulation results demonstrate good performance in terms of the insertion loss in the pass band, and a good shape factor. A comparison between different results depends on the S-parameters was presented. This comparison showed the optimum way to design a substrate-integrated waveguide using LTCC technology.

References

[1] Y. Rong, K. A. Zaki, M. Hageman, D. Stevens, and J. Gipprich, "LTCC ridge waveguide bandpass chip filters," IEEE Transactions on Microwave Theory and Techniques, Vol. 47, No. 12, pp. 2317-2324, 1999.

[2] J. A. Ruiz-Cruz, Y. Zhang, K. A. Zaki, A. J. Piloto, and J. Tallo, "Ultra-wideband LTCC ridge waveguide filters," IEEE Microwave and Wireless Components Letters, Vol. 17, No. 2, pp. 115-117, 2007.

[3] H. Grubinger, H. Barth, and R. Vahldieck, "An LTCC-based 35-GHz substrate-integrated-waveguide bandpass filter," Paper presented at the IEEE International Microwave Symposium, Boston, MA, pp. 1605-1608, 2009.

[4] R. Valois, D. Baillargeat, S. Verdeyme, M. Lahti, and T. Jaakola, "LTCC technology for 40 GHz bandpass waveguide filter," Microwave Symposium Digest, DOI: 10.1109/MWSYM.2005.1516783, pp. 953-956, 2005.

[5] F. Yang and H. Yu, "Two novel substrate integrated waveguide filters in LTCC," IEEE International Conference on Millimeter Wave Technology, ICMMT, pp. 229-232, 2010.

[6] H. Chien, T. Shen, T. Huang, W. Wang, and R. Wu, "Miniaturized band-pass filters with double-folded substrate integrated waveguide resonators in LTCC," IEEE Transactions on Microwave Theory and Techniques, Vol. 57, No. 7, pp. 1774-1782, 2009.

[7] G. Lee, C. Yoo, J. Yook, and J. Kim, "SIW quasi-elliptic filter based on LTCC for 60 GHz application," 4th European Microwave Integrated Circuits Conference, pp. 204-207, 2009.

[8] L. Wu, X. Zhou, and W. Yin, "A novel multilayer partial H-plane filter implemented with folded substrate integrated waveguide," IEEE Microwave and Wireless Components Letters, Vol. 19, No. 8, pp. 494-496, 2009.

[9] B. Schulte, V. Ziegler, B. Schoenlinner, U. Prechtel, and H. Schumacher, "Miniaturized KU-band filters in LTCC technology—Evanescent mode vs. standard cavity filters," 40th European Microwave Conference, pp. 1700-1703, 2010.

[10] B. Chen, T. Shen, and R. Wu, "Dual-band vertically stacked laminated waveguide filter design in LTCC," IEEE Transactions on Microwave Theory and Techniques, Vol. 57, No. 6, pp. 1554-1562, 2009.

[11] Y. Konishi, and K. Uenakada, "The design of a band pass filter with inductive strip-planar circuit mounted in waveguide," IEEE Transactions on Microwave Theory and Technology, Vol. 22, pp. 869-873, 1974.

[12] R.E. Collin, "*Field Theory of Guided Waves*," McGraw-Hill, New York, 1960.

[13] G.L. Matthaei, L. Young, and E.M.T. Jones, "*Microwave Filters, Impedance-Matching Network, and Coupling Structures*," McGraw-Hill, New York, 1964.

[14] Dupont 9K7 green-tape data sheet, "http://www2.dupont.com/MCM/en_US/assets/downloads/prodinfo/GreenTape9K7DataSheet.pdf," *DuPont Company*, accessed Jan. 1st, 2011.